Single-Photon Counting Detector Scalability for High Photon Efficiency Optical Communications Links

Brian E. Vyhnalek, Jennifer N. Downey, and Sarah A. Tedder

National Aeronautics and Space Administration
Glenn Research Center
Cleveland, OH, USA

ABSTRACT

For high photon-efficiency deep space or low power optical communications links, such as the Orion Artemis-2 Optical Communications System (O2O) project, the received optical signal is attenuated to the extent that single-photon detectors are required. For direct-detection receivers operating at 1.55 μm wavelength, single-photon detectors including Geiger-mode InGaAs avalanche photon diodes (APDs), and in particular superconducting nanowire single-photon detectors (SNSPDs) offer the highest sensitivity and fastest detection speeds. However, these photon detectors exhibit a recovery time between registered input pulses, effectively reducing the detection efficiency over the recovery interval, resulting in missed photon detections, reduced count rate, and ultimately limiting the achievable data rate. A method to overcome this limitation is to divide the received optical signal into multiple detectors in parallel. Here we analyze this approach for a receiver designed to receive a high photon efficiency serially concatenated pulse position modulation (SCPPM) input waveform. From measured count rate and efficiency data using commercial SNSPDs, we apply a model from which we determine the effective detection efficiency, or blocking loss, for different input signal rates. We analyze the scalability of adding detectors in parallel for different modulation orders and background levels to achieve desired data rates. Finally we show tradeoffs between the number of detectors and the required received optical power, useful for real link design considerations.

Keywords: Optical communications, single photon detectors, superconducting nanowire, few-mode fibers

1. INTODUCTION

Several upcoming NASA missions will be featuring optical communications capabilities, such as the Laser Communication Relay Demonstration (LCRD)[1] providing all-optical high-rate communications from geostationary orbit, the Orion Artemis-2 Optical Communications System project (O2O), (formerly Orion EM-2),[2] an 80 - 250 Mbps direct-to-Earth link capability for the crewed mission aboard the Orion Multi-Purpose Crew Vehicle (OMPCV) from lunar distances, and the Deep Space Optical Communication (DSOC) Project,[3] a demonstration of laser communications flight transceiver and ground receiver technology from 0.1-2 astronomical units (AU), to be hosted aboard the Psyche Mission spacecraft.[4] In particular the O2O and DSOC missions will make use of the Consultative Committee for Space Data Systems (CCSDS) Optical Communications High Photon Efficiency (HPE) Standard,[5] and require photon-counting receivers. While the upcoming optical communication demonstrations will continue to validate capabilities, considerations are also being given to cost-effective ground terminal technologies that are both scalable and assembled from commercial-off-the-shelf (COTS) components. Ideally a system could be designed that could support a variety of data rates, telescope aperture sizes, and environmental factors such as background light and atmospheric turbulence levels. In this paper we focus on commercial fiber-coupled superconducting nanowire single photon detectors (SNSPDs) as part of a real-time photon counting optical communications receiver system. We show measured characteristics, and discuss how these parameters can be used to effectively model and simulate a PPM communications system with SNSPDs. Finally we give an example link scenario to show how depending on data rate and other system parameters, we can determine the required number of detectors to close the link error-free with a specified link margin.

Send correspondence to brian.e.vyhnalek@nasa.gov

2. SINGLE-PHOTON DETECTORS

In a direct-detection optical communication system the basic receiver architecture consists of a telescope aperture for light collection and focusing, and a photosensitive surface that converts the detected optical intensity into an electrical signal. For photon-starved links, such that the transmitted laser power is reduced to a few photons per signal period at the receiver, single-photon detectors must be used. At near-IR wavelengths, in particular 1.55 μm, the highest sensitivity, lowest noise, and fastest detectors currently available are superconducting nanowire single photon detectors (SNSPDs), which must operate at cryogenic temperatures. Options for coupling to cryogenic SNSPDs are either through fiber-optic, or free-space coupling, but both can present challenges for efficiency and scalability. Here we consider the detector system depicted in Figure 1. In this case the light collected from the receive aperture is fiber-coupled, and split to multiple individual fiber-coupled SNSPDs. The splitting can be accomplished using standard fiber splitters, however photonic lanterns can potentially offer a higher coupling efficiency solution.[6,7] As will be further discussed in Section 3, this approach can offer design flexibility for different data rates and link conditions. However, first we will describe the detector characteristics important for receiver modeling and link assessment.

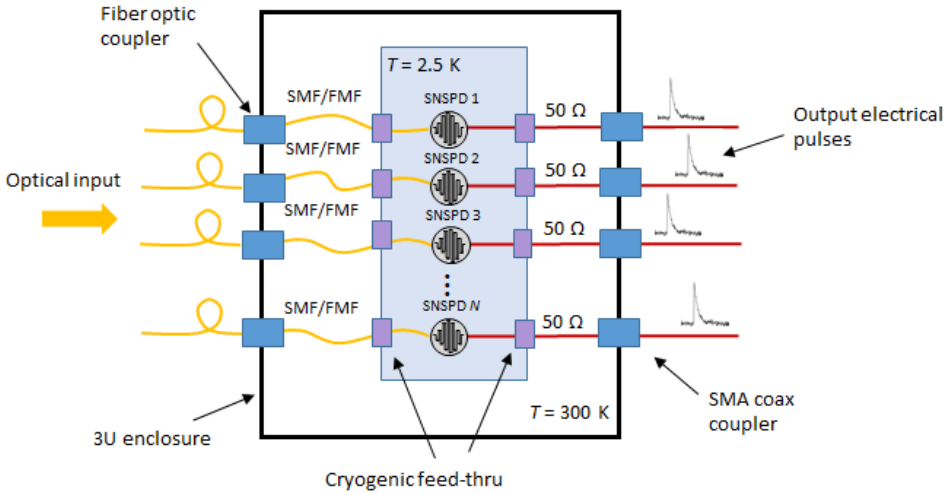

Figure 1: Fiber-coupled multichannel single-photon detector system.

2.1 Detector Characteristics

Previously we have characterized a commercial 2.5 K SNSPD system in terms of detection efficiency, dark-count rate, dead time, and timing jitter for different fiber coupling and readout circuit configurations.[8,9] Specifically fiber coupling with both standard telecom single mode fiber, SMF-28, as well as 20-μm graded-index (GRIN) 6-mode few mode fiber (FMF), and readout circuits in which the preamplifier stage is either AC-coupled or DC-coupled. Here we repeat this characterization at 1.55 μm operating wavelength for four additional SNSPDs. In this case each of the detectors are optically coupled to 20-μm GRIN FMF, however three of the detectors have been designed with a modified superconducting layer for higher intrinsic absorption and reduced sensitivity to longer wavelengths, hence greater blackbody rejection. Additionally each of the fibers coupling to the detectors have been coated with an anti-reflection (AR) layer to further reduce dark counts due to blackbody radiation. Finally, the electrical readout circuits of each of the detectors are DC-coupled to reduce the nonlinear interaction between the circuit and detector, allowing for higher-speed operation.[10]

In Figures 2a-2d we show the results of this characterization. The standard style detector is labeled as Ch 1, whereas the detectors with modified design are labeled as Ch 2, 3, and 4 throughout. Figure 2a shows single-shot oscilloscope traces of the SNSPD response pulses output through two 500 MHz, 25 dB gain room temperature low noise amplifiers. For this measurement the detectors were biased at the fraction of their respective switching currents I_{SW}, $I_{B,1} \approx 0.86 I_{SW,1}$, $I_{B,2} \approx 0.92 I_{SW,2}$ and $I_{B,3,4} \approx 0.95 I_{SW,3,4}$ such that each had approximately

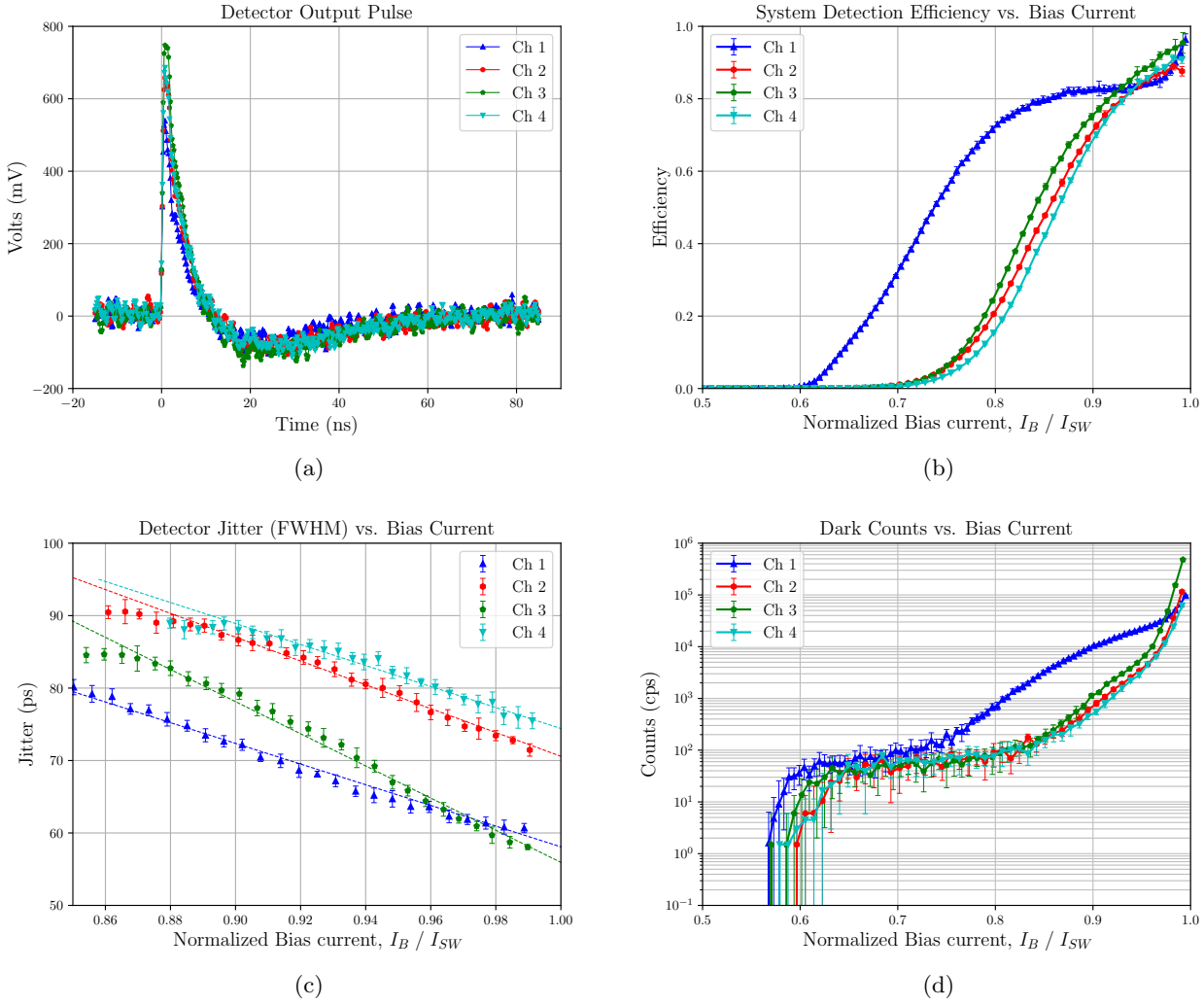

Figure 2: (a) Detector electrical output pulses. (b) System Detection Efficiency (SDE) as a function of bias current. (c) Detector timing jitter (FWHM) for varying bias current. (d) Dark count rate dependence on bias current.

identical operating points with detection efficiency ≈ 80%, background/dark count rate ≈ 3000 cps, and FWHM jitter ≈ 75 - 80 ps. The response pulses for each detector are nearly identical except for pulse height, with Ch 1 displaying a noticeably reduced amplitude of ≈ 550 mV, compared with the ≈ 650 - 750 mV pulse heights of Ch 2 - 4. Regardless, for each detector the rising edge was ≈ 850 ps, however determination of the decay time presented an ambiguity due to the ≈ 100 mV negative dip in the response curves. This slight bipolar response is not intrinsic to the SNSPDs, and can be attributed to filtering present on the signal introduced by the readout electronics.

Detection efficiency measurements are shown in Figure 2b, and dark counts in Figure 2d as a function of bias current. In this case the detection efficiency is referenced to the fiber coupler input ports on the detector system enclosure, as depicted in Figure 1, hence the efficiency is referred to as the system detection efficiency (SDE) since it includes the additional losses due to fiber coupling. Similarly, the dark counts considered are the photon counts measured with the input laser off, and a blackout curtain covering the detector system. For

each detector the SDE curves exhibited characteristic sigmoid-type behavior with Ch 1 showing a well-defined plateau at $\approx 82\% \pm 1.2\%$, whereas this effect was suppressed in Ch 2 - 4 owing to the thicker superconducting layer. Note that typical meander SNSPDs have polarization dependent efficiency, and the plots shown are for the best polarization. When configured for the worst polarization, the SDE for each channel is reduced by $\approx$ 2 dB. From Figure 2d it can be seen that the corresponding dark count rate is $\approx$ 1 - 3 kcps for all channels at the $SDE = 80\%$ point. Previous measurements near the 80% efficiency levels with SMF-coupled devices[8] showed a dark count rate of < 100 cps, whereas FMF-coupled devices without additional filtering saw $\approx$ 10 - 30 kcps.[9] Based on the prior measurements with FMF-coupling, the newer AR-coated FMFs provide nearly 10 dB improvement in blackbody reduction.

Figure 2c shows the measured detector jitter for varying bias currents. The detection jitter was determined by illuminating the SNSPDs with attenuated 1.55 μm, 100 femtosecond, 50 MHz pulses and measuring the histogram of the time differences between the emitted pulses and photon counts. This histogram is the instrument response function (IRF), which was determined to have a Gaussian profile. The values shown in Figure 2c are the full width at half maximum (FWHM) of the measured IRFs, which range from $\approx$ 60 ps - 80 ps in the best cases and accounts for the added jitter from the measurement system. Since detector jitter is the dominant source of timing jitter in single-photon counting systems, this can be a constraining factor such as for PPM high photon efficiency optical communications in which the RMS timing jitter should be less than 10% of the slot width.[5] The corresponding measured RMS jitter is in the range of $\approx$ 25 - 34 ps, which is well below the 50 ps requirement of a 0.5 ns slot width, however 0.25 ns and 0.125 ns slot widths may be limiting.

2.2 Count Rate and Blocking Losses

Due to the microscopic detection mechanisms particular to a single-photon detector, the detector will exhibit the property of reduced or inactive operation for a period of time after a detection event. For free-running APDs the positive feedback in the impact ionization dynamics requires external gating electronics, or avalanche quenching circuitry which can limit achievable count rates to low MHz. Similarly, in SNSPDs the hot spot dissipation dynamics and material kinetic inductance limit count rates to the 10s of MHz in the highest efficiency material systems. In Figure 3 we plot the measured output counts vs. estimated input photon flux when illuminated

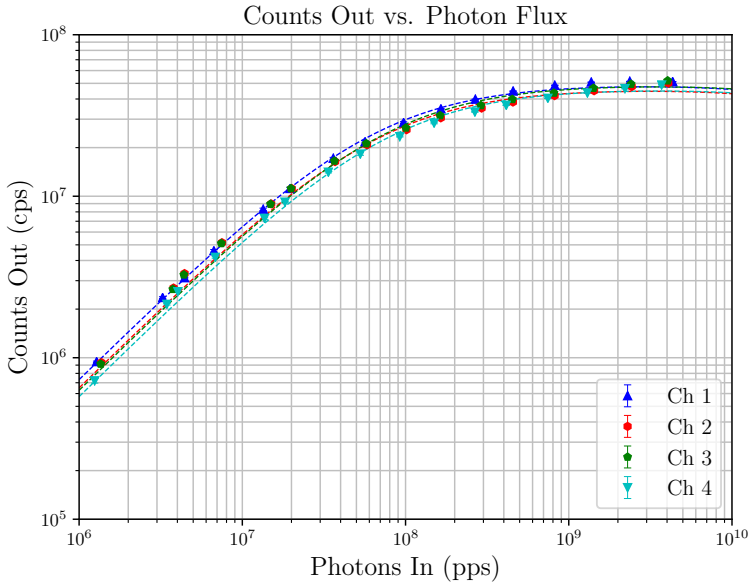

Figure 3: Output count rate vs. input photon flux.

from a continuous wave (CW) 1.55 μm laser. From the plot it can be seen that the output count rates increase

nearly linearly until ≈ 20 Mcps for about 30 - 40 M-photons/s input flux, and ultimately saturate to about 60 Mcps at nearly 1 G-photon/s flux rate. Also for each detector channel we fit the curve defined by

$$n_{out}(N) = \frac{pN}{p - 1 + e^{pN\tau}}, \tag{1}$$

where N is the input photon flux, τ is the $1/e$ detector reset time, and p is a fitting parameter, $p \in [0, 1]$, from which we extract the detector reset time. From the curve fits, we estimate τ to be on the order of $\tau \approx 12$ - 15 ns, which correspond to an equivalent 90%/10% reset time of 26 - 32 ns.

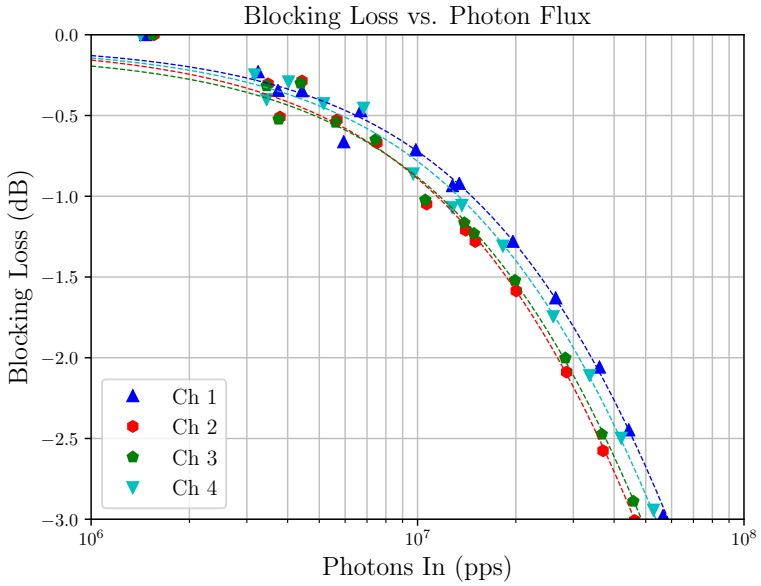

Figure 4: Blocking loss dependence on input photon flux rate.

From the measured count rates we can also determine the blocking loss as a function of input flux. Blocking loss, as shown in Figure 4, refers to the count rate reduction incurred from missed counts due to the finite detector reset time. Equivalently, we can consider the blocking loss as a reduction in detector efficiency from the low-flux maximum, in this case 82%, resulting in an effective efficiency that is flux dependent. Hence, in Figure 4 the -1 dB blocking loss point corresponds to an effective 65% detection efficiency, the -2 dB blocking loss point corresponds to an effective 52% detection efficiency, etc. Blocking loss is one of the main limiting factors for achieving high data rate optical communications with single-photon detectors. As will be discussed next, by simply splitting the signal between multiple detectors and aggregating the output counts, blocking losses can be mitigated and higher data rates accessed. However, there are still limitations to this approach, depending on the received photon flux and fiber coupling strategies.

3. RECEIVER SCALABILITY AND LINK ASSESSMENT

Multiple parallel fiber-coupled single-photon detectors can offer a flexible and potentially cost-saving approach to ground terminal design for a variety of laser communication link scenarios. In particular, using commercially available detectors modularly added as required to sufficiently receive a downlink signal can reduce recurring costs associated with redesign and customization to meet various mission requirements. Similarly, the commercial-off-the-shelf (COTS), and relatively low complexity of this approach can enable smaller, potentially portable, and a larger number of ground terminals, overcoming the limited availability of large astronomical telescopes and also increasing site diversity. While large apertures and custom, dedicated instrumentation will still be needed for the most extreme cases and ambitious links, the COTS photon-counting approach can be particularly enabling

for future SmallSat and CubeSat missions using optical communications, especially for deep space,[11] university level optical and quantum communications, and commercial interests.

3.1 Photon Counting Simulation

To accurately determine the number of detectors in parallel needed receive a downlink signal we simulate a simplified photon detection and counting process for different PPM signals and data rates. The inputs are wavelength λ, modulation order M, slot period T_s, average received photons per slot $K_{s,in}$, transmitter extinction ratio α, average received background photon flux rate n_b, maximum detection efficiency η_{max}, $1/e$ reset time τ, dark count rate n_{dark}, RMS detection jitter σ_J, maximum number of detectors N_d, and total number of symbols simulated N_{sym}. Simulations are performed by first generating N_{sym} symbols of length $M + M/4$, where the additional $M/4$ slots is to account for guard slots where no signal is present, and assigning a signal slot randomly drawn from a uniform distribution on the interval $[0, M-1]$. Next, for each detector, every slot in a symbol is assigned a random number of photons drawn from a Poisson distribution, where the average number input into the distribution is dependent on whether the slot is a signal or non-signal slot. Figure 5 depicts a schematic of this process.

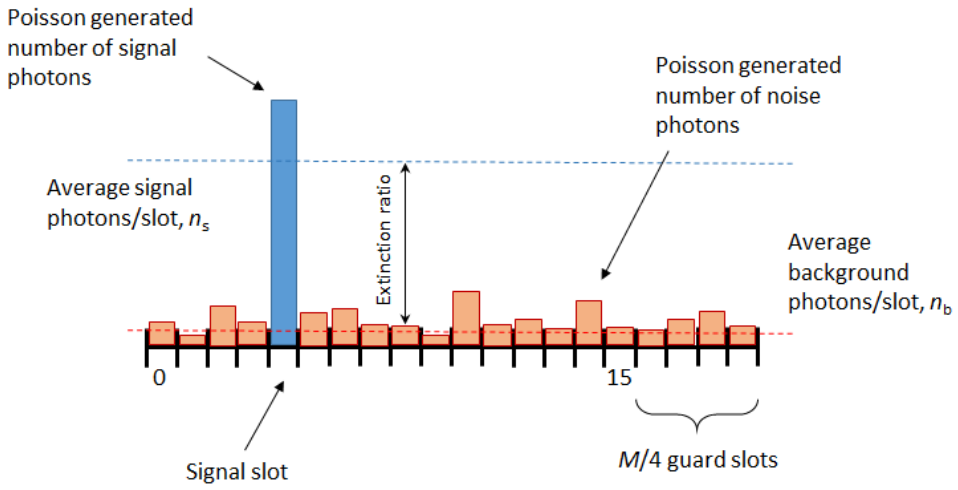

Figure 5: Signal and noise photon distribution for a single 16-PPM symbol.

For a non-signal slot, we calculate the average number of photons per slot per detector $k_{b,in}$, from the received background flux, dark count rate, number of detectors, extinction ratio and input signal. It follows that

$$k_{b,in} = \frac{1}{N_d T_s} \left(n_b + \alpha K_{s,in} + N_d n_{dark} \right) \tag{2}$$

Extinction ratio is very important since depending on the signal power, photons present in non-signal slots due to the non-ideal laser 'off' state can contribute significantly to the received noise photon flux. Similarly, for a signal slot the average number of photons per slot per detector $k_{s,in}$, is given by

$$k_{s,in} = \frac{1}{N_d T_s} \left(n_b + T_s K_{s,in} + N_d n_{dark} \right), \tag{3}$$

since the received background and thermally generated blackbody photons are present at all times. However, for a signal slot this can be beneficial since the single-photon detector cannot discriminate between a signal or noise photon. Once the number of photons per slot per detector have been realized, we assign random arrival times to each photon. Within a signal slot the photon arrival time distribution is determined by the pulse shape, hence could be Gaussian or some other profile, but for simplicity we assume a square pulse equal to the slot period thus the arrival times are uniformly distributed over the interval $[mT_s, (m+1)T_s]$, where m is the slot index.

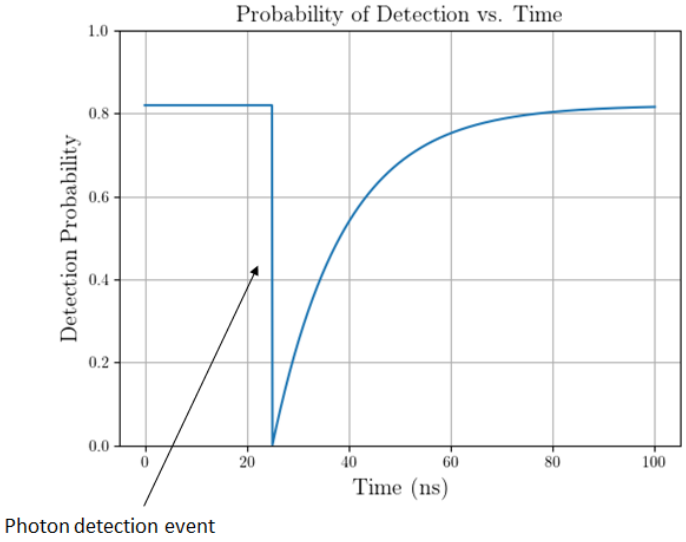

Figure 6: Illustration of modeled SNSPD detection probability vs. time.

We simulate detection events and incorporate detector reset effects as follows. Since the photon detection efficiency is effectively the probability to detect an incident photon, for each detector and for each photon in a slot with arrival time t_i, we generate a uniformly distributed random number r between 0 and 1 and check if $r \leq \eta(t_i)$, where $\eta(t)$ is the time dependent detection probability given by

$$\eta(t) = \eta_{max}\left(1 - e^{-(t-t_0)/\tau}\right) \tag{4}$$

with t_0 being the timestamp of the most recent detection event. If $r \leq \eta(t_i)$ we regard that photon as detected. To incorporate the effects of detector jitter we set $t_0 = t_i + t_j$, where t_j is a normally distributed random number with mean $\mu = \sigma_J/2$, and variance $\sigma^2 = \sigma_J^2$. Figure 6 illustrates the time dependent detection probability, where we see the probability at a constant maximum of 0.82 until 25 ns where a photon detection event occurs. The probability instantaneously goes to zero, and then recovers according to Equation 4. Theoretically it will take an infinite amount of time for $\eta(t) = \eta_{max}$ after a detection has occurred, thus for numerical purposes we set $\eta(t) = \eta_{max}$ when $\eta(t) \geq 0.98\eta_{max}$. Also, at high enough flux rates SNSPDs will go into a state of sustained oscillation before fully latching. We incorporate this limiting phenomena by assigning a maximum photon inter-arrival time for which no detections can occur, in this case 8 ns. Finally, for each detector we individually add up the number of detected photons per signal slot k_s, and noise slot k_b, separately, which we then sum across all the detectors to determine the aggregate detected signal photons K_s, and noise photons K_b.

3.2 Example: 267 Mbps Link Assessment

Using values of detector parameters derived from the characterization measurements we give an example of a link assessment. In this case we consider a relatively high data rate 267 Mbps link. The corresponding modulation parameters are $M = 16$, slot width $T_s = 0.5$ ns, code rate $r = 2/3$. A complete list of the simulation parameters are given in Table 1. Note that the maximum number of detectors N_d considered here is 32, since this is the maximum number of COTS SNSPDs that can be fit onto a single standard 2.5 K cryogenic cold head. In Figure 7a we plot the capacity and SCPPM performance curves for $K_b = 0$ and $K_b = 0.01$. From these curves we can see that in order to close the link error-free in the $K_b = 0.01$ worst case, we require a K_s/M count of $\geq\approx$ -9.8 detected dB-signal photon/slot. In Figure 7b we show the output of the photon detector simulations for the detected signal photons per slot. The total detected noise photons per slot in all cases is $K_b < 0.001$.

Parameter	Value
λ	1.55 μm
M	16
T_s	0.5 ns
$K_{s,in}$	$\{1, 2, 4, 8, 16, 32\}$ ph/pulse
α	0.0001
n_b	100 kHz
η_{max}	82%
τ	15 ns
n_{dark}	3 kHz
σ_J	30 ps (rms)
N_d	32
N_{sym}	100,000

Table 1: Simulation parameters for 267 Mbps link example.

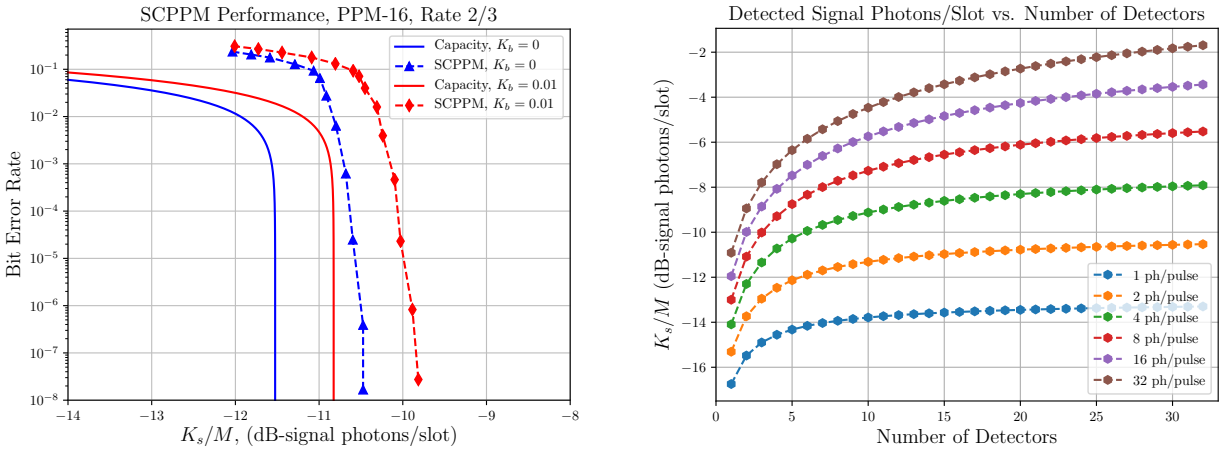

(a) (b)

Figure 7: (a) SCPPM performance for PPM-16, code rate 2/3 for background photon count levels $K_b = 0$ and $K_b = 0.01$. (b) Detected dB-signal photons per slot, K_s/M vs. the number of detectors for different received signal photons per slot, $K_{s,in}$.

Although the SCPPM performance curve gives a required $K_s.M$ of $\approx$ -9.8 detected dB-signal photon/slot we must also account for jitter and other implementation losses in the receiver. Assuming a value of -2 dB for receiver implementation loss[12] gives a target value without margin of $\approx$ -7.8 detected dB-signal photon/slot. From Figure 7b we see that this can be achieved with a few different combinations, namely with 32 received photons per signal pulse and 3 detectors, 16 photons per signal pulse and 5 detectors, 8 photons per signal pulse and 8 detectors, or very nearly 4 photons per pulse and 32 detectors. A limitation that these curves indicate is that there are diminishing returns at lower photon levels as the number of detectors increases and the signal is split.

In a real link scenario we would need to operate with some level of margin over the required level to account for inaccuracies in the assumed link parameters. For the 8 received photons per pulse case adding up to 32 detectors gives $\approx$ 2.3 dB of additional margin, for 16 photons per pulse we get $\approx$ 4.4 dB and for 32 photons and 32 detectors we can achieve $\approx$ 6.2 dB margin. For this analysis we have been implicitly assuming a single receiver aperture feeding into multiple fiber coupled detectors. Without assuming specific aperture sizes or fiber coupling

scenarios, if we assume instead multiple apertures with multiple fiber coupled detectors, the curves plotted in Figure 7b can be considered the detected signal photons per slot *per aperture*. Therefore it follows that through aperture arraying it would be possible to obtain performance gains and increased margin for lower numbers of received photons and detectors per aperture by the same factor. Table 2 illustrates this by showing an simplified example link budget for two receiver scenarios - Case A, a single 60 cm receiver aperture, and Case B an array of four 40 cm apertures.

	Case A	Case B
Tx power	400 mW	400 mW
Tx aperture	22 cm	22 cm
Tx ideal gain	112.65 dB	112.65 dB
Tx efficiency	-6.2 dB	-6.2 dB
Range	4×10^5 km	4×10^5 km
Space loss	-310.22 dB	-310.22 dB
Atmospheric loss	-1.0 dB	-1.0 dB
Rx aperture	60 cm	40 cm
Rx ideal gain	121.70 dB	118.18 dB
Rx efficiency	-10.0 dB	-10.0 dB
Rx dB-ph/s	92.12 dB	88.53 dB
Rx signal ph/pulse	16.29	7.13
Rx array gain	0.0 dB	6.0 dB
Number of detectors (per aperture)	32	4
Detected K_s/M (per aperture)	-3.38 dB	-9.46 dB
Detected K_b (per aperture)	0.0008	0.0002
Required K_s/M	-7.8 dB	-7.8 dB
Margin	4.42 dB	4.34 dB

Table 2: Sample link budget for 267 Mbps from lunar distances.

4. CONCLUSION

We measured detection efficiency, dark-count rate, reset time, timing jitter and blocking loss on commercial SNSPDs optically coupled with 20-μm FMF, and designed with a modified superconducting layer for higher intrinsic absorption and reduced sensitivity to longer wavelengths. The fibers were also coated with an anti-reflection (AR) layer to further reduce dark counts due to blackbody radiation. At the optimal operating point, the detection efficiency was $\approx$ 82%, with dark count rates $\approx$ 3 kcps, and detection jitter $\approx$ 60 - 80 ps FWHM. Blocking losses were found to be $\approx$ 3 dB for input photons fluxes on the order of 40 - 50 Mph/s, indicating detector reset times on the order of 14 - 15 ns ($1/e$). We developed a photon counting model and simulation to accurately account for detector reset time and jitter for PPM photon counting optical communications. From these measured detector parameters we assessed the detector requirements and scalability for a 267 Mbps link. Finally we showed that depending on certain link parameters, there are several options for the number of COTS detectors required in parallel depending on the available receiver aperture options. With a scalable approach using commercial parts, future missions with optical communications capability will be increasingly enabled.

ACKNOWLEDGMENTS

The authors would like to acknowledge the support by the NASA Space Communications and Navigation (SCaN) program.

REFERENCES

[1] Luzhanskiy, E., Edwards, B., Israel, D., Cornwell, D., Staren, J., Cummings, N., Roberts, T., and Patschke, R., "Overview and status of the laser communication relay demonstration," in [*Free-Space Laser Communication and Atmospheric Propagation XXVIII*], Hemmati, H. and Boroson, D. M., eds., **9739**, 100 – 113, International Society for Optics and Photonics, SPIE (2016).

[2] Robinson, B. S., Shih, T., Khatri, F. I., Boroson, D. M., Burnside, J. W., Guldner, O., Constantine, S., Torres, J., Yarnall, T. M., DeVoe, C. E., Hubbard, W., Geisler, D. J., Stevens, M. L., Mikulina, O., Spellmeyer, N. W., Wang, J. P., Butler, R., Hogan, M., King, T., and Seas, A., "Laser communications for human space exploration in cislunar space: ILLUMA-T and O2O," in [*Free-Space Laser Communication and Atmospheric Propagation XXX*], Hemmati, H. and Boroson, D. M., eds., **10524**, 231 – 235, International Society for Optics and Photonics, SPIE (2018).

[3] Biswas, A., Srinivasan, M., Piazzolla, S., and Hoppe, D., "Deep space optical communications," in [*Free-Space Laser Communication and Atmospheric Propagation XXX*], Hemmati, H. and Boroson, D. M., eds., **10524**, 242 – 252, International Society for Optics and Photonics, SPIE (2018).

[4] Oh, D. Y., Collins, S., Goebel, D., Hart, B., Lantoine, G., Snyder, S., Whiffen, G., Elkins-Tanton, L., Lord, P., Pirkl, Z., and Rotlisburger, L., "Development of the Psyche Mission for NASA's Discovery Program," in [*35th International Electric Propulsion Conference*], Georgia Institute of Technology (October 2017).

[5] Consultative Committee for Space Data Systems (CCSDS), *Optical Communications Coding and Synchronization Recommended Standard, 142.0-B-1 Blue Book* (2019).

[6] Birks, T. A., Gris-Sánchez, I., Yerolatsitis, S., Leon-Saval, S. G., and Thomson, R. R., "The photonic lantern," *Advances in Optics and Photonics* **7**, 107 – 167 (2015).

[7] Tedder, S. A., Vyhnalek, B. E., Leon-Saval, S., Betters, C., Floyd, B., Staffa, J., and Lafon, R., "Single-mode fiber and few-mode fiber photonic lanterns performance evaluated for use in a scalable real-time photon counting ground receiver," in [*Free-Space Laser Communications XXXI*], Hemmati, H. and Boroson, D. M., eds., **10910**, 69 – 78, International Society for Optics and Photonics, SPIE (2019).

[8] Vyhnalek, B. E., Tedder, S. A., and Nappier, J. M., "Performance and characterization of a modular superconducting nanowire single photon detector system for space-to-Earth optical communications links," in [*Free-Space Laser Communication and Atmospheric Propagation XXX*], Hemmati, H. and Boroson, D. M., eds., **10524**, 369 – 377, International Society for Optics and Photonics, SPIE (2018).

[9] Vyhnalek, B. E., Tedder, S. A., Katz, E. J., and Nappier, J. M., "Few-mode fiber coupled superconducting nanowire single-photon detectors for photon efficient optical communications," in [*Free-Space Laser Communications XXXI*], Hemmati, H. and Boroson, D. M., eds., **10910**, 62 – 75, International Society for Optics and Photonics, SPIE (2019).

[10] Kerman, A. J., Rosenberg, D., Molnar, R. J., and Dauler, E. A., "Readout of superconducting nanowire single-photon detectors at high count rates," *Journal of Applied Physics* **113**(14), 144511 (2013).

[11] Shelton, M., Pulkkinen, A., Summerlin, E. J., and Storm, M., "SETH Technology Demonstration of Small Satellite Deep Space Optical Communications to aid Heliophysics Science and Space Weather Forcasting," in [*Proceedings of the AIAA/USU Conference on Small Satellites*], SSC19-P3-17 (2019).

[12] Downey, J. N., Vyhnalek, B. E., Tedder, S. A., , and Lantz, N. C., "Detector channel combining results from a high photon efficiency optical communications link test bed," in [*Free-Space Laser Communications XXXII*], International Society for Optics and Photonics, SPIE (2020).